Bioactive Materials 12 (2022) 314–326

Contents lists available at ScienceDirect

Bioactive Materials

journal homepage: www.keaipublishing.com/en/journals/bioactive-materials

# Cyanobacteria-based self-oxygenated photodynamic therapy for anaerobic infection treatment and tissue repair

Bailiang Wang [a,b,1], Liyang Zhou [a,b,1], Yishun Guo [a,b], Hanwen Guo [a,b], Yiming Zhong [a,b], Xiaomin Huang [a,b], Yifan Ge [a,b], Qingying Wang [a,b], Xiaoying Chu [a,b], Yingying Jin [a,b], Kaiyue Lan [a,b], Mei Yang [a,b], Jia Qu [a,b,*]

[a] School of Ophthalmology and Optometry, Eye Hospital, School of Biomedical Engineering, Wenzhou Medical University, Wenzhou, 325000, PR China
[b] Research Group of Advanced Ophthalmology Bionic Interface Materials, Oujiang Laboratory, Wenzhou, 325000, PR China

ARTICLE INFO

*Keywords:*
Refractory keratitis
Periodontitis
Anaerobic infection
Self-oxygenated
Photodynamic therapy

ABSTRACT

Photodynamic therapy (PDT) is an important technique to deal with drug-resistant bacterial infections in the post-antibiotic era. However, the hypoxic environment in intractable infections such as refractory keratitis and periodontitis, makes PDT more difficult. In this work, spontaneous oxygen-producing cyanobacteria were used as the carrier of photosensitizer (Ce6), and ultrasmall $Cu_{5.4}O$ nanoparticles ($Cu_{5.4}O$ USNPs) with catalase activity for infection and inflammation elimination and rapid tissue repair (CeCycn-$Cu_{5.4}O$). The loading of Ce6 and $Cu_{5.4}O$ USNPs onto cyanobacteria surface were confirmed by transmission electron microscopy, nano particle size analyzer, scanning electron microscopy. *In vitro* sterilization and biofilm removal experiments demonstrated that the restriction of hypoxic environment to PDT was significantly alleviated due to the oxygen production of cyanobacteria. Under laser irradiation, the close transfer of energy photons to oxygen produced by cyanobacteria reduced more than 90% of Ce6 dosages (660 nm, 200 mW/cm$^2$, 2 min). It is worth mentioning that both rapid sterilization through PDT and long-term oxidized free radicals elimination were achieved by adjusting the ratio of Ce6 and $Cu_{5.4}O$ USNPs. Both periodontitis and refractory keratitis animal models proved the excellent self-oxygenation enhanced antibacterial property and promotion of tissue repair.

## 1. Introduction

Currently, antibiotics are main effective means of bacterial infections treating with development cycle far behind the time of bacterial resistance generation [1]. According to speculations from the World Health Organization (WHO), by 2050, 10 million people will die every year from diseases caused by bacterial resistance [2]. No drugs will be available to treat infectious diseases caused by superbugs. Especially, it is extremely difficult to achieve tissue repair and wound closure for chronic inflammatory wounds accompanied by bacterial infections [3–5]. The main reason is the immune system response caused by infections, including immune cell attack and oxidative stress mediated by the sustained release of inflammatory mediators, *etc.* [6–10] However, the development of bacterial resistance, bacterial biofilm formation and the hiding of bacteria in immune cells are the crucial reasons for the failure of bacteria elimination through immune system. Bacteria even turn immune cells into refuge and resist the ablation of immune cells through changing their phenotype and secreting specific enzymes [11,12]. The most difficult and common problem of bacterial infection is the formation of bacterial biofilm, which cause physical isolation to antibacterial agents, as well as a series of changes in its genotype and survival status. In terms of human pathogenic bacteria, anaerobic pathogenic bacteria cause refractory oral cavity, keratitis, upper respiratory tract and diabetic foot, *etc.*, which are the most difficult infections to cure [13,14].

In response to such a severe situation of drug resistance, scientific researchers and clinicians have joined forces to develop a series of new sterilization materials and sterilization strategies [15,16]. New

Peer review under responsibility of KeAi Communications Co., Ltd.
* Corresponding author. School of Ophthalmology and Optometry, Eye Hospital, School of Biomedical Engineering, Wenzhou Medical University, Wenzhou, 325000, PR China.
*E-mail address:* jqu@wz.zj.cn (J. Qu).
[1] These authors contributed equally to this work.

https://doi.org/10.1016/j.bioactmat.2021.10.032
Received 31 July 2021; Received in revised form 14 October 2021; Accepted 20 October 2021
Available online 30 October 2021
2452-199X/© 2022 The Authors. Publishing services by Elsevier B.V. on behalf of KeAi Communications Co. Ltd. This is an open access article under the CC BY-NC-ND license (http://creativecommons.org/licenses/by-nc-nd/4.0/).

sterilization strategies include responsive or controllable drug delivery systems [17], reversible sterilization-bacterial corpse release surface [18–21], targeted sterilization in immune cells [22,23], *etc*. Novel sterilization materials include light-to-heat conversion materials, photocatalytic sterilization materials, chemical catalytic sterilization materials, and biologically extracted active sterilization active ingredients and so on [24,25]. Among them, photocatalytic sterilization is currently the most studied sterilization mode owing to its obvious advantages such as broad-spectrum sterilization, not causing drug resistance, and controllable implementation process [26–28]. Photodynamic sterilization requires indispensable three basic elements, photosensitizer, oxygen and light source. During the PDT process, photosensitizer is excited by the light, and oxygen molecules absorb the photoelectrons generated in the excited state to generate singlet oxygen and other oxidative free radicals [29–31]. As a result, sufficient oxygen supply in the photocatalysis process is a key factor in the overall therapeutic effect especially for anaerobe-related infections treatment.

The effect of photodynamic therapy could be improved through increasing oxygen supply, especially for tumors and chronic infections and other highly hypoxic environments [32–34]. The ways to increase the oxygen supply are mainly divided into three ways: nanomaterials carrying oxygen, in-situ catalysis of hydrogen peroxide to generate oxygen, and algae oxygen generation under light irradiation. Comparing with the first two oxygen supply methods, algae oxygen supply has obvious advantages such as high biocompatibility and continuous oxygen supply. For example, Min Zhou developed an oxygen-generating system through microalgae-mediated photosynthesis to relieve hypoxic environment in tumors [35]. The engineered living microalgae could be delivered to hypoxic tumor regions to increase local oxygen levels and re-sensitize resistant cancer cells to both radio- and phototherapies. Jian Ji developed two-step sequential delivery strategy using perfluorohexane (PFH)-loaded liposomes (lip) as oxygen ($O_2$) and commercial antibiotics carriers [36]. It was found that the quorum sensing and the drug efflux pumps of bacteria are suppressed by restraining related gene expression as the relief of hypoxia, leading to the reduced antibiotic resistance. However, one-time medication is difficult to completely solve the infection problem especially for long-term chronic infections treatment. Long-term chronic inflammation is the physiological basis leading to immune system attack and wound non-healing [37,38]. It is well known that infection elimination, oxidative stress and inflammatory removal are indispensable requirements for tissue repair.

As for the elimination of oxidative stress damage and inflammation caused by infection, the main problem of hormones and anti-inflammatory drugs using is the cumulative toxicity and side effects [39,40]. Once bacterial infections happen, inflammatory factors, chemokines and other cytokines are produced in large quantities that further cause gradient immune cells attacks and oxidative stress for bacterial infections elimination. However, once the bacterial infection persists, the infected wound will stagnate in the pro-inflammatory M1 state. The immune cells and oxidative stress damage continue to attack bacteria leaving the wounds into a stand-off state which further promote drug-resistant bacteria multiplication [41]. Rapid photodynamic sterilization combined with oxidative stress elimination is considered to be a more effective strategy for wound repair than simple bacteria sterilization [42]. Fortunately, the development of nano-enzyme technology in recent years has provided us with new option to reduce oxidative stress damage and the accompanying inflammatory response [43]. Nano-enzymes with high-efficiency catalase activity such as Pt, $MnO_2$, nano-iridium and ultra-small copper clusters could quickly degrade reactive oxygen species (ROS) into harmless water and oxygen [44,45]. In comparison, ultra-small copper nanoclusters showed high enzyme activity which could be obtained by a simple reduction method [46].

In this work, cyanobacteria were simultaneously used to load Ce6 and $Cu_{5.4}O$ USNPs to construct a novel synergistic functional system against anaerobic infections (CeCyan-$Cu_{5.4}O$). The morphology and oxygen production performance of the modified cyanobacteria were measured by scanning electron microscope and dissolved oxygen meter. The effect of oxygen production on photodynamic generation of free radicals, bacteria elimination, and bacterial biofilm removal performance was verified in detail. The combination of $Cu_{5.4}O$ USNPs was precisely tuned so as to ensure the bactericidal effect of ROS generation during photodynamic therapy (PDT). The relief of hypoxia was explored with hypoxia fluorescent probe and dissolved oxygen meter. The inflammatory factors and microenvironment changes were explored using two hypoxic infection models, refractory cornea and periodontitis. Hence, this self-oxygenated cyanobacteria-based PDT and inflammation elimination system provides an attractive approach for refractory anaerobe infection treatment.

## 2. Materials and methods

### 2.1. Materials

Lithium phenyl-2,4,6-trimethybenzoylphosphinate (LAP), ascorbic acid, copper chloride (II), Gelatin methacryloyl (GelMA) (65% graft degree), 4-Arm PEG Amine ($M_W = 2000$), Cyanobacteria Synechococcus elongatus PCC 7942 strain was obtained from Freshwater Algae Culture Collection at the Institute of Hydrobiology (FACHB), Chinese Academy of Sciences (CAS). Menadione, L-Cysteine hydrochloride monohydrate, Hemin and Yeast extract were purchased from Shanghai Aladdin Biochemical Technology (China), Amino PEG Amine ($M_W = 400$) was purchased from Pensure Biological (China). Trypticase Soy Broth (TSB) was obtained from Beijing Land Bridge Technology (China). BHI Broth was purchased from Qingdao Hope Bio-Technology (China). Chlorin e6 (Ce6) was obtained from Shanghai Macklin Biochemical (China). Human corneal epithelial cells (HCECs) and mouse fibroblasts cells (L-929) were purchased from American type culture collection (USA). Bacteria including *Streptococcus gordonii* (*S. Gordonii*, ATCC 10558), *Propionibacterium acnes* (*P. gingivalis*, ATCC 33277), *Fusobacterium nucleatum* (*F. nucleatum*, ATCC 10953) and *Porphyromonas gingivalis* (*P. acnes*, ATCC 6919) were obtained from Shanghai biosource collection center (China). Penicillin and Streptomycin were purchased from Gibico BRL (USA). A CCK-8 assay kit and LIVE/DEAD™ Cell Viability/Cytotoxicity Kit for mammalian cells were obtained from Thermo Fisher Scientific (USA). LIVE/DEAD BacLight Bacterial Viability Kit was obtained from Invitrogen (USA). All immunofluorescence related reagents were purchased from Abcam (USA).

### 2.2. Synthesis and characterization of CeCyan

CeCyan was synthesized by the following procedures. Firstly, the carboxyl group contained in the photosensitizer Ce6 was aminated. Ce6 (2 mg/mL dissolved in 1 mL DMSO) and of 1-Ethyl-3-(3dimethylaminopropyl) carbodiimide (EDC) (1 mg/mL dissolved in 1 mL DMSO) were dropwise added to 100 μL polyethylene glycol solution ($NH_2$-PEG-$NH_2$, $M_w = 400$ Da) in 10 mL DMSO. Afterwards, the mixture was stirred for 6 h under dark conditions for fully mixing and amination of Ce6. After the reaction, dialysis was performed with a molecular weight cutoff of 1000 Da to remove unreacted substances to purify amino-modified Ce6. The absorbance of the purified amino-modified Ce6 was measured at 402 nm to calculate the concentration. The cyanobacteria culture solution was centrifuged at 6000 rpm for 6 min and the supernatant was removed. PBS (pH 5.0) was added to reconstitute the cyanobacteria solution. Then the absorbance at 730 nm was measured to calculate the cyanobacteria concentration. Amino-modified Ce6 was added to the cyanobacteria solution, that was mixed on a shaker for 2 h in the dark. After combination, the final product CeCyan was obtained through 6000 rpm centrifugation for 6 min.

### 2.3. Fabrication and simulated enzyme catalytic performance of $Cu_{5.4}O$ USNPs

#### 2.3.1. Fabrication of $Cu_{5.4}O$ USNPs

$Cu_{5.4}O$ USNPs was synthesized through following procedures [46]. Firstly, 20 mM $CuCl_2$ powder was dissolved in 100 mL ultrapure water and stirred in an oil bath at 80 °C for 10 min. Then 200 mM of L-ascorbic acid was completely dissolved in 100 mL of ultrapure water. After that, L-ascorbic acid was slowly added dropwise to the $CuCl_2$ solution and cooled to room temperature under stirring conditions. The pH of the solution was adjusted to 8.0–9.0 with 1 M NaOH. The mixture was continuously stirred in an oil bath at 80 °C for 12 h. After the reaction, large-volume particles were removed by centrifugation (8000 g, 15 min), and then the supernatant was dialyzed with pure water for two days (*Mw* cutoff: 7000). After purification, the product was concentrated using a vacuum concentrator.

The $Cu_{5.4}O$ USNPs was combined with 4-arm PEG-$NH_2$ to enhance dispersion. 1 mL of 17.5 μg/mL $Cu_{5.4}O$ USNPs was ultrasonically oscillated for 20 min and the Zeta potential was measured. After 100 μL of 4-arm PEG-$NH_2$ (*Mw* = 2000) was added and stirred for another 24 h, unreacted 4-arm PEG-$NH_2$ molecules were removed by dialysis (*Mw* cutoff: 3500). Then the Zeta potential was measured to verify the surface modification process. The copper concentration in the solution was measured by ICP.

#### 2.3.2. The $H_2O_2$ scavenging activity of $Cu_{5.4}O$ USNPs

The $H_2O_2$ scavenging ability of $Cu_{5.4}O$ USNPs was tested using Hydrogen Assay Kit (Beyotime, China). Ferric ions could be oxidized by hydrogen peroxide to form a purple product with an absorption peak at 560 nm. Then, different concentrations of $Cu_{5.4}O$ USPS at 91.25–1460 ng/mL and 50 μM $H_2O_2$ were incubated at 37 °C for 2 h. Upon completion of the reaction, the remaining $H_2O_2$ concentration was measured as per the manufacturer's instructions to calculate the $H_2O_2$ scavenging ability.

#### 2.3.3. The superoxide dismutase (SOD)-like activity of $Cu_{5.4}O$ USNPs

The SOD-like activity of $Cu_{5.4}O$ USNPs was determined by formazan formation using Total Superoxide Dismutase Assay Kit with NBT (Beyotime, China). In short, Xanthine Oxidase (Xanthine Oxidase) oxidized xanthine to produce $O^{2-}$ which then converted nitroblue tetrazolium (NBT) to NBT formazan with a characteristic absorption at 560 nm. The formazan concentration at 560 nm was measured by microplate reader. In brief, a series of $Cu_{5.4}O$ USNPs samples at different concentrations were blended with a reaction solution containing xanthine, xanthine oxidase and NBT, and incubated at 37 °C for 30 min. Concentration of NBT formazan produced was measured as per the manufacturer's instructions to count the percentage of inhibition.

#### 2.3.4. The glutathione peroxidase (GPx)-like activity of $Cu_{5.4}O$ USNPs

The GPx-like activity of $Cu_{5.4}O$ USNPs was evaluated by using Glutathione Peroxidase Assay Kit (Beijing Leagene Biotechnology, China). Glutathione (GSH) can react with 5,5′-Dithiobis-2nitrobenzoic acid (DTNB) to form a compound with a characteristic absorption at 422 nm, which can be monitored using a microplate reader. During the test, GSH was catalyzed by the oxidant and $Cu_{5.4}O$ USNPs to oxidized glutathione (GSSG). The decrease of GSH concentration was proportional to the catalytic activity of $Cu_{5.4}O$ USNPs. The GPx-like activity was measured as per the manufacturer's instructions at 422 nm.

### 2.4. In vitro assessment of $O_2$ and reactive oxygen species (ROS) generation

The $O_2$ production was measured by the JPB-607A portable dissolved oxygen meter. In short, dissolved oxygen concentration was measured under increasing concentrations of cyanobacteria ($2 \times 10^7$, $4 \times 10^7$, $6 \times 10^7$ cells/mL) and light intensities (0, 100, 200, 300 mW/$cm^2$) every minute. All experiments were carried out under the room temperature of 25 °C, pH 7.4. The data were averaged after repeating the experiment for at least six times.

Dichloro-dihydro-fluorescein diacetate (DCFH-DA) (40 μL, 10 mM) and 20 μL of sodium hydroxide (2 M) were added into 18 mL of deionized water. DCFH was hydrolyzed from DCFH-DA by shaking the mixture at room temperature for 30 min in the dark. After that, 2 mL of Tris buffer (100 mM, pH 7.2) was added to terminate the reaction, so 20 mL of DCFH stock solution (20 μM) was obtained and stored in the dark at −4 °C before use. DCFH-DA was selected as the chemically ROS probe. 20 μM of DCFH stock solution was mixed with the CeCyan or CeCyan-$Cu_{5.4}O$ solutions with different concentrations at 1:1 and 1:2 respectively to ensure the concentration of the DCFH probe is within the working concentration of 5–10 μM. The mixtures were irradiated under a 660 nm laser at 200 mW/$cm^2$. The fluorescence absorbance at 525 nm was recorded every minute with a microplate reader for 10 min, and compared with the initial value to calculate the fluorescence enhancement.

### 2.5. In vitro cell studies

#### 2.5.1. Cell cultures

Human corneal epithelial cells (HCECs) and mouse fibroblasts cells (L-929) were cultured in DMEM/F12 (Gibico, America) and DMEM (Gibico, America) cell culture medium with 10% of fetal bovine serum (FBS) and 1% of penicillin-streptomycin (10000 U/mL Penicillin and 10000 U/mL of Streptomycin, Gibico, America) at Cell culture incubator (37 °C, 5% $CO_2$).

#### 2.5.2. Assessment of cytocompatibility

The cell viability was evaluated using CCK-8 assay kit and LIVE/DEAD assay kit according to the manufacturer's instructions. First, HCEC and L-929 were seeded in 96-well plates at a density of 10000 cells per well and 5000 cells per well respectively. After 24 h, observed the adherence of the cells under a microscope, and added CeCyan-$Cu_{5.4}O$ solutions of different concentrations (concentrations of Ce6 was 0.625, 1.25, 2.5, 5, 10, 20 μg/mL). After incubation for 4 h, the culture medium was removed and washed with PBS for 2–3 times. Then, 100 μL of 10% CCK-8 solution was added to each well. The orifice plate continued to be cultured in the cell incubator. After 2–4 h, the absorbance at 450 nm was measured with a microplate reader (SpectraMax 190, Molecular Devices LLC, United States).

LIVE/DEAD™ Cell Viability/Cytotoxicity Kit were also used to determine biocompatibility towards mammalian cells. The cells were inoculated and cultured for 24 h in accordance with above methods. Then, CeCyan-$Cu_{5.4}O$ solution was added at different concentrations (0.625, 1.25, 2.5, 5, 10, 20 μg/mL, respectively) for another 24 h incubation. The cells were washed twice with PBS to remove culture medium. After washing, 100 μL of CalceinAm/PI working solution was added to each well. The cells were washed twice with PBS to remove the dyes after 30 min incubation in the dark. The images of the stained cells were observed using an inverted fluorescence microscope (DMi8, Leica Microsystems).

### 2.6. In vitro antibacterial experiment

#### 2.6.1. Bacterial culture

The most common four kinds of anaerobes *S. Gordonii*, *P. gingivalis*, *F. nucleatum* and *P. acnes* were selected as the model bacterial to evaluate the antibacterial or anti-biofilm properties of CeCyan-$Cu_{5.4}O$. All of the four bacterial species were commercially obtained from Shanghai biosource collection center (Shanghai, China). Four bacteria were cultured in different media and anaerobic environment according to their growth needs. For instance, *P. Gingivalis* were cultivated in trypticase soy broth (TSB, Land Bridge) supplemented menadione (1 mg/L, Aladdin), L-cysteine hydrochloride (0.5 g/L, Aladdin), yeast extract (5 g/

L, Aladdin), hemin (5 mg/L, Aladdin). Additional 8% of aseptic defibrillated sheep blood anaerobically with 80% of $N_2$, 10% of $H_2$ and 10% of $CO_2$. *F. Nucleatum* and *P. acnes* were cultivated in trypticase soy broth (TSB, Land Bridge) supplemented menadione (1 mg/L, Aladdin), L-cysteine hydrochloride (0.5 g/L, Aladdin), yeast extract (5 g/L, Aladdin) and hemin (5 mg/L, Aladdin) anaerobically with 80% $N_2$, 10% $H_2$ and 10% $CO_2$. *S. Gordonii* was cultured aerobically in brain-heart infusion broth (BHI Broth, Hopebio) supplemented menadione (1 mg/L, Aladdin), L-cysteine hydrochloride (0.5 g/L, Aladdin), yeast extract (5 g/L, Aladdin) and hemin (5 mg/L, Aladdin).

#### 2.6.2. Bactericidal properties of CeCyan-$Cu_{5.4}O$

The bactericidal properties of CeCyan-$Cu_{5.4}O$ against the anaerobic bacteria through plate counting method. Specially, *P. gingivalis* ($10^7$ colony forming units (CFU)/mL), *F. nucleatum*($10^5$ CFU/mL) and *P. acnes* ($10^7$ CFU/ml) were added to 96-well plates (100 μL), then divided into the such groups as blank control group, Ce6+L group, Ce6+$Cu_{5.4}O$ + L group, Cyan-$Cu_{5.4}O$ + L group, CeCyan + L group, CeCyan(death)+L group, CeCyan-$Cu_{5.4}O$ group, and CeCyan-$Cu_{5.4}O$ + L group (L means irradiated under a 660 nm laser at 200 mW/$cm^2$, 2 min). The different components in each group were Ce6 at 5 μg/mL, Cyan at 1 × $10^8$ CFU/mL, and $Cu_{5.4}O$ at 182.5 ng/mL. The treated bacterial solution was diluted and spread on an anaerobic agar plate, and cultured under anaerobic conditions for 24–48 h. Finally, the number of bacterial colonies were used to calculate the change in the bacteria concentration and the sterilization efficiency.

#### 2.6.3. Bacterial biofilm cultivation and elimination of CeCyan-$Cu_{5.4}O$

As for the formation of *P. gingivalis* and *P. acnes* single-species biofilm, bacteria were inoculated at a concentration of $10^8$ CFU/mL in 24-well plates. All biofilm were cultured in conditioned medium at 37 °C for 96 h. The culture medium was changed every 24 h, and a total of 4 d culture was sufficient to form mature periodontal biofilm.

The prepared bacterial biofilm was treated by different methods in the following groups including blank control group, $Cu_{5.4}O$ + L control group, Cyan + $Cu_{5.4}O$ + L control group, Ce6+L group, Ce6+$Cu_{5.4}O$ + L group, Cyan + $Cu_{5.4}O$ + L group, Cyan + $Cu_{5.4}O$ + L group, and CeCyan + $Cu_{5.4}O$ + L group (L means irradiated under a 660 nm laser at 200 mW/$cm^2$). The concentration of Ce6 in CeCyan-$Cu_{5.4}O$ could be converted into 10 μg/mL. To distinguish the living and dead of bacteria within the biofilm, the biofilm was stained with a mixture of SYTO 9 (2.5 μM) and propidium iodide (2.5 μM) (Live/Dead Baclight Bacterial Viability Kit). After fully washing the dyes, bacterial biofilm was imaged with Confocal laser microscope (CLSM, Germany).

### 2.7. Animal studies of the antibacterial properties

#### 2.7.1. Anaerobic bacteria infection animal model and administration method

Sprague Dawley (SD) rats (180–200 g, 6 weeks) were obtained from Shanghai Jiesjie Laboratory Animal Co. LTD. China. Both anaerobic infectious keratitis and infectious periodontitis animal models were established after adaptive feeding for one week. All the experimental animals involved were kept in the Experimental Animal Center of Wenzhou Medical University in compliance with the Code of Conduct for the Care and Use of Experimental Animals. This experiment was approved by the Experimental Animal Ethics Review Committee of Wenzhou Medical University.

In order to increase the retention time of CeCyan-$Cu_{5.4}O$ in the lesion, the GelMA-based hydrogel was used to incorporate the CeCyan-$Cu_{5.4}O$. Specially, 0.6 g of GelMA was dissolved in 4 mL of DPBS at 50 °C. The prepared CeCyan solution was dissolved in GelMA solution to form homogeneous solution. Then, $Cu_{5.4}O$ USNPs solution was added and stirred to be fully dispersed (200 rpm, 10 min). Then, 0.45 mg lithium phenyl-2, 4, 6 trimethylbenzoyl phosphinate (LAP) was added to the solution as photoinitiator after stirring (200 rpm, 10 min). Subsequently, the solution was poured in a customized mold and cured using LED lights with a spectrum width of 385–515 nm to obtain the injectable hydrogel. The microstructure of GelMA hydrogel and CeCycn-$Cu_{5.4}O$ GelMA hydrogel were evaluated by SEM. Before scanning, the uncross-linked sample was dropped on the surface of the silicon wafer to photo-crosslink into glue and freeze-dried. The cross section was cut off and coated with Au–Pd to take SEM images.

#### 2.7.2. Anaerobic infectious keratitis

The SD rats were randomly divided into 4 groups with 5 rats in each group. During the experiment, rats were anesthetized by intraperitoneal injection of chloral hydrate. Before inoculation to *P. acnes*, the rat corneal epithelium was scraped to increase the chance of infection. Rats in all groups were treated with 20 μL of *P. acnes* ($10^8$ CFU/mL) in the right eye and the eyelids were sutured to create an anaerobic environment. The left eye of each rat was served as an unvaccinated control.

After inoculation, the rats were checked 2–3 times a day, and another 20 μL *P. acnes* ($10^8$ CFU/mL) was used to treat the wound every 24 h. Keratitis appeared within 72 h after inoculation through examination using a slit lamp biological microscope. After successful anaerobic infectious keratitis formation, the rats were divided into the following groups, including CeCyan-$Cu_{5.4}O$ in GelMA hydrogel, CeCyan in GelMA hydrogel, Levofloxacin in GelMA hydrogel, and no treating group. After wearing the contact lens, 660 nm laser was applied to irradiate the antibacterial materials for 2 min except for the contact lens containing levofloxacin. The contact lens was worn continuously for 30 min every day for 3 days. While levofloxacin was applied twice a day for 3 days. The wound secretions were scraped and dissolved in 2 mL of PBS. Then the concentration of bacteria was calculated through counting the colonies after coating 50 μL of the bacteria solution onto plate and overnight culture.

#### 2.7.3. Anaerobic infectious periodontitis

Twenty SD rats were randomly divided into 4 groups with 5 rats in each group. In short, daily subgingival injections of lipopolysaccharide (1 mg/mL, 0.02 mL) and mixed bacteria (*S. Gordonii*, *P. gingivalis* and *F. nucleatum*, 1:1:1, $10^8$ CFU/mL, 0.02 mL) were injected into the subgingival area of the mandibular incisor. After a total of 3 d modeling, the rats were divided into the following groups including CeCyan-$Cu_{5.4}O$ in GelMA hydrogel, CeCyan in GelMA hydrogel, Levofloxacin in GelMA hydrogel, and no treatment. The CeCyan-$Cu_{5.4}O$ and CeCyan groups were irradiated with 660 nm laser for 2 min, washed with PBS solution after half an hour. The treatment was applied treated once a day for 3 days. The levofloxacin group was treated twice a day for 3 days.

#### 2.7.4. Evaluation of treatment effects

The ocular surface and gingiva of rats were observed and photographed by biological slit lamp microscope, and scored based on the degree of inflammation. At the same time, the secretions from the eye or gingival lesion were collected and coated onto bacterial culture plate to calculate the changes of bacteria number in the infected site. Finally, the corneal tissues and gingival tissues were removed from the euthanized animals at the last day. Then, hematoxylin and eosin (H&E) staining and fluorescence immunostaining were used to observe the inflammation level of the infected sites.

### 2.8. Statistical analysis

All data were expressed as mean ± standard deviation. SPSS was used for statistical analysis. A value $p < 0.05$ was considered statistically significant.

## 3. Results and discussion

### 3.1. Fabrication and characterization of CeCyan-$Cu_{5.4}O$

The aim of this work was to construct self-oxygenated PDT system against refractory anaerobic infections based on cyanobacteria which were used as both continuous oxygen production reactor and drug carrier (Scheme 1). It is worth mentioning that the close-range combination of Ce6 and cyanobacteria could greatly promote the ability of oxygen molecules to undertake energy photon into oxygen free radicals. Aiming at the highly complex etiology and microenvironment of the tissue area infected by refractory anaerobes, efficient sterilization, bacterial biofilm removal, continuous oxygen supply, elimination of oxidative stress and inflammation are considered to be a brand-new treatment mode. In this strategy, the procedural treatment mechanism of rapid sterilization under light, biofilm removal and efficient elimination of ROS was realized by adjusting the ratio of the bactericidal component (Ce6) and the oxidative stress removal component ($Cu_{5.4}O$ USNPs). Furthermore, the $O_2$ generation of cyanobacteria could enhance the sensitivity anaerobic bacteria to antibiotics. Continuous oxygen supply was also beneficial to tissue repair and new blood vessel growth in refractory skin infection wounds. As for refractory anaerobic infections of tissues in the optical path of the eye, the increase in oxygen supply in this area could avoid the inflammation damage to the tissues and reduce the production of new blood vessels.

The Cyan strain is an original freshwater single-cell microorganism, usually cultured in BG11 medium (Blue Green Medium) with 20 mW/$cm^2$ indoor light [47]. Cyan is a kind of photosynthetic autotrophic gram-negative bacteria, containing chlorophyll in cytoplasm as the photon collection center, so it appears green in daylight. Due to the presence of chlorophyll, cyanobacteria can act as a PDT center to photosynthesize and continuously provide oxygen. As showed in Fig. 1A and **B**, the shape and size of Cyan were firstly examined through optical microscope and SEM. The Cyan strain was rod-shaped with 0.6–1.0 μm in width and 4.0–6.0 μm in length on average [48]. To confirm the combination of Ce6 and $Cu_{5.4}O$ USNPs onto the Cyan surface, surface charge properties of Cyan cells before and after drugs loading were verified through Zeta potentials testing (Fig. 1C). The outer membrane was negatively charged in the aqueous solution, allowing low-polarity and positively charged substances to pass through [49]. The surface charge of Ce6 changed from highly negatively charged into positively charged after aminated modification. The surface charge of Cyan changed from negatively charged into nearly neutral after surface modification of Ce6–$NH_2$. The amount of Ce6 loaded on Cyan cells could be obtained by deducting the Ce6 content in the centrifugal supernatant. The concentration of Ce6 solution could be calculated through drawing the standard absorbance curve of Ce6 at 402 nm (Fig. S1). Although surface charge of $Cu_{5.4}O$ was close to neutral after surface hydrophilization treatment by 4-arm PEG-$NH_2$. The $Cu_{5.4}O$ USNPs was combined onto Cyan mainly based on van der Waals forces and hydrogen bonds, *etc* [46,48].

The UV/Vis spectra of CeCyan cells also proved the successfully loading of Ce6 onto the Cyan surface (Fig. 1D). Surface amination of –$NH_2$ onto Ce6 and surface combination of Ce6 onto Cyan did not change its original structure. The ROS generation of CeCyan cells under 660 nm laser irradiation was examined and compared with free Ce6 and amide-functionalized Ce6 using a commercial ABDA and DCFH-DA kit (Fig. 1E and **F**). There was no DCFH-fluorescence absorbance for DCFH as control, 0.3 μg/mL Ce6, 0.435 μg/mL CeCyan cells without laser irradiation. When 660 nm laser irradiation was applied on the 3.0 μg/mL Ce6, obvious DCFH-fluorescence absorbance was detected indicating the generation of ROS in several minutes. It was also found that the increase of Ce6 amount loaded onto Cyan from 0.317 μg/mL to 0.589 μg/mL greatly enhanced DCFH-fluorescence absorbance. It was surprised to find that ROS generation in free Ce6 group (3.0 μg/mL) was even lower than that in CeCyan group (0.317 μg/mL), which meant about 90% dosage reduction of Ce6 using. This phenomenon could be attributed to reason that the energy electrons generated from the excited photosensitizer could be accepted by the oxygen produced by the cyanobacteria to generate ROS [50]. Therefore, the existence of the oxygen-generating carrier significantly reduced the energy loss from the light energy to the chemical energy. The effects of Cyan concentration and laser power on

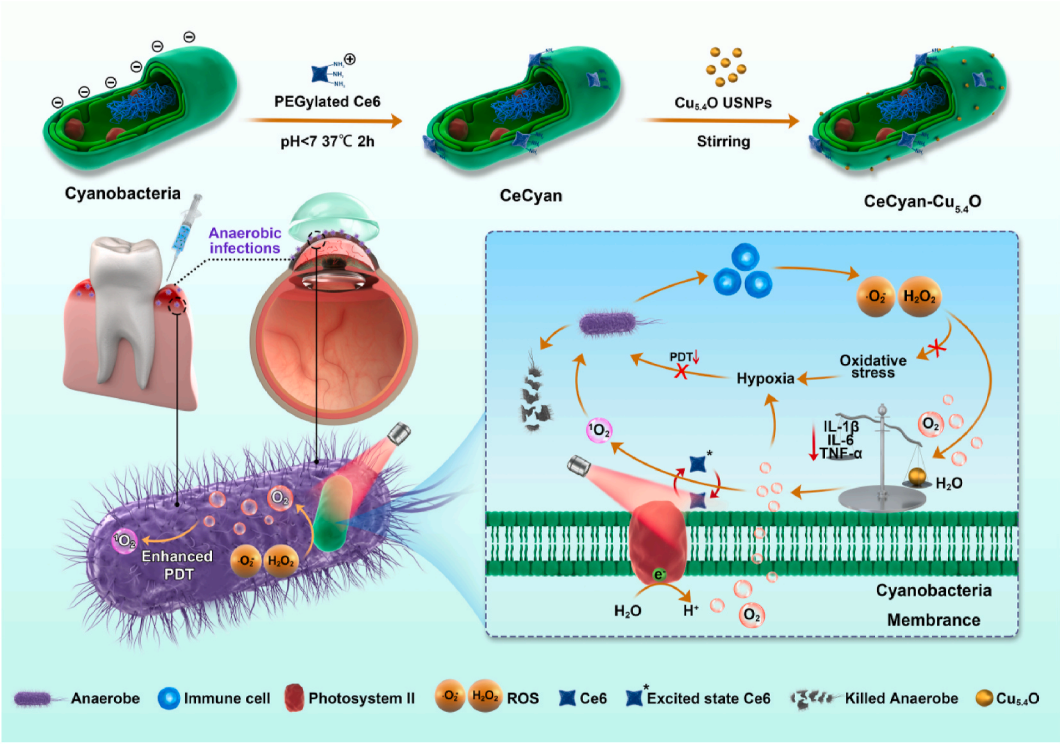


**Scheme 1.** Schematic illustration of the fabrication of CeCyan-$Cu_{5.4}O$ and application in treating of anaerobic bacteria infection.

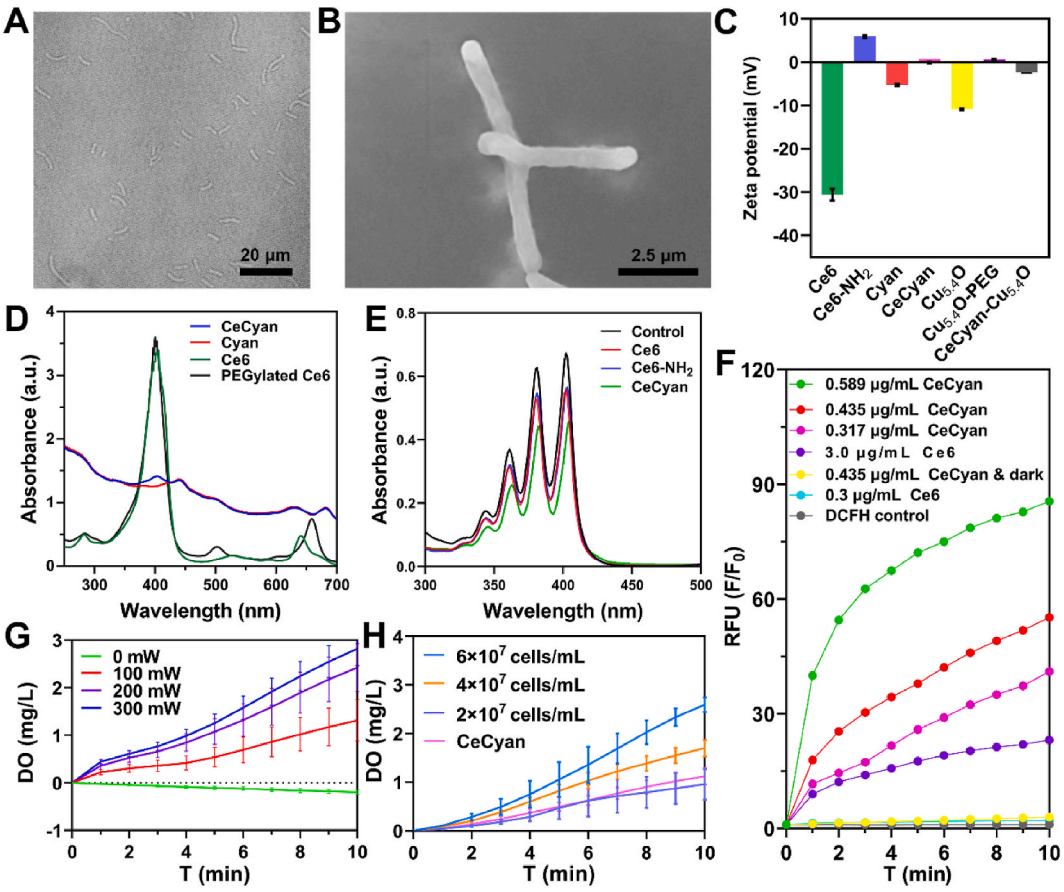


**Fig. 1. Fabrication of CeCyan-$Cu_{5.4}O$ and the oxygen generation performance. (A)** Optical microscope of Cyan cells. **(B)** Scanning electron microscope image of Cyan cells. **(C)** Zeta potentials of Cyan cells, Ce6, amide-functionalized Ce6, CeCyan cells, $Cu_{5.4}O$ USNPs and PEGylated $Cu_{5.4}O$ USNPs. **(D)** UV/Vis spectra of CeCyan cells, Cyan cells, free Ce6 and PEGylated Ce6. **(E)** UV/Vis spectra of Ce6-([Ce6] = 0.5 μg/mL), amide-functionalized Ce6-([amide-functionalized Ce6] = 0.5 μg/mL) and CeCyan-([Ce6] = 0.5 μg/mL; [Cyan] = $5 \times 10^6$ cells/mL) based photodynamic outcomes using ABDA as the probe (under 660 nm, 200 mW/$cm^2$ irradiation for 2 min). **(F)** Relative DCFH-fluorescence intensities of CeCyan cells ([Cyan] = $4 \times 10^7$ cells/mL) and Ce6 at varied concentrations under 660 nm, 200 mW/$cm^2$ laser irradiation. **(G)** Dissolved oxygen level of the Cyan cells solution under 660 nm laser irradiation at increased power for 10 min ([Cyan] = $4 \times 10^7$ cells/mL). **(H)** Oxygenation ability of Cyan cells at varies concentration and CeCyan cells ([Cyan] = $4 \times 10^7$ cells/mL) under 660 nm laser irradiation.

oxygenation were also studied through recording the changes of solution turbidity. It was found that the increase of Cyan concentration and power both significantly increased the production of oxygen (Fig. 1G and **H**). In order to investigate the effect of GelMA coating on the oxygen production of Cyan, we immersed Cyan ($1 \times 10^8$ cells/mL) coated within GelMA in PBS, and compared the oxygen production with the same amount of free Cyan solution under the same light environment. As shown in Fig. S3, the Cyan coated with GelMA still presented good oxygen production function. In the following experiments, CeCyan cells containing 0.317 μg/mL Ce6 were chosen unless there was special explanation.

### 3.2. *Enzyme-like catalytic activity of $Cu_{5.4}O$ USNPs*

Inflammation and oxidative stress damage are natural immune process against pathogen infection. Oxidative stress is related to both acute and chronic inflammations. However, excessive uncontrolled inflammation can lead to delayed wounds healing or diseases cure. Immune deficiencies or metabolic diseases of the body can easily lead to protracted chronic infections and development of bacterial biofilm, which further stimulate and aggravate the inflammatory response and oxidative stress damage in the wound. As a result, a synergistic functional treatment strategy that combines high-efficiency sterilization, bacterial biofilm removal, and elimination of oxidative stress damage is considered a better choice. Nanozymes is one kind of nanomaterials with enzymatic catalytic properties such as glucose oxidase, peroxidase, catalase, superoxide dismutase and others [51]. In this study, a newly reported $Cu_{5.4}O$ USNPs with large surface area volume ratio as nanozymes was combined onto CeCyan cells to alleviate the inflammatory after refractory anaerobe infections elimination.

The $Cu_{5.4}O$ USNPs were synthesized through reduction of $Cu^{2+}$ by L-ascorbic acid (AA) [46]. The TEM image of the obtained $Cu_{5.4}O$ USNPs was shown Fig. 2A, with an average size ~5.4 nm. The obtained SEM and Mapping images of CeCyan-$Cu_{5.4}O$ are shown in Fig. 2B and S4. It can be seen that $Cu_{5.4}O$ USNPs successfully adsorbed on the surface of cyanobacteria. The tricky problem in the system is how to realize that the ROS generated during PDT treatment will not be cleared by $Cu_{5.4}O$ USNPs. The concentration of $Cu_{5.4}O$ USNPs loaded onto cyanobacteria is the key point, which should not significantly reduce the bactericidal and biofilm elimination during PDT treatment. After that, $Cu_{5.4}O$ USNPs can also effectively play ROS scavenging effects after that. As showed in Fig. 2C and Fig. S2, CeCyan cells displayed no nanozyme catalytic property. The loading of $Cu_{5.4}O$ USNPs exhibited obvious ROS scavenging effect that led to the reduction of ROS concentration. At the same time, it was also found that the increase of Cu concentration (182.5 ng/mL, 365 ng/mL and 730 ng/mL) did not further significantly reduce the amount of ROS production. Therefore, it believed that CeCyan--$Cu_{5.4}O$ would exert good bactericidal effect just through extending the radiation time, increasing the ratio of Ce6 to Cu or raising the radiation intensity to further enhance PDT property.

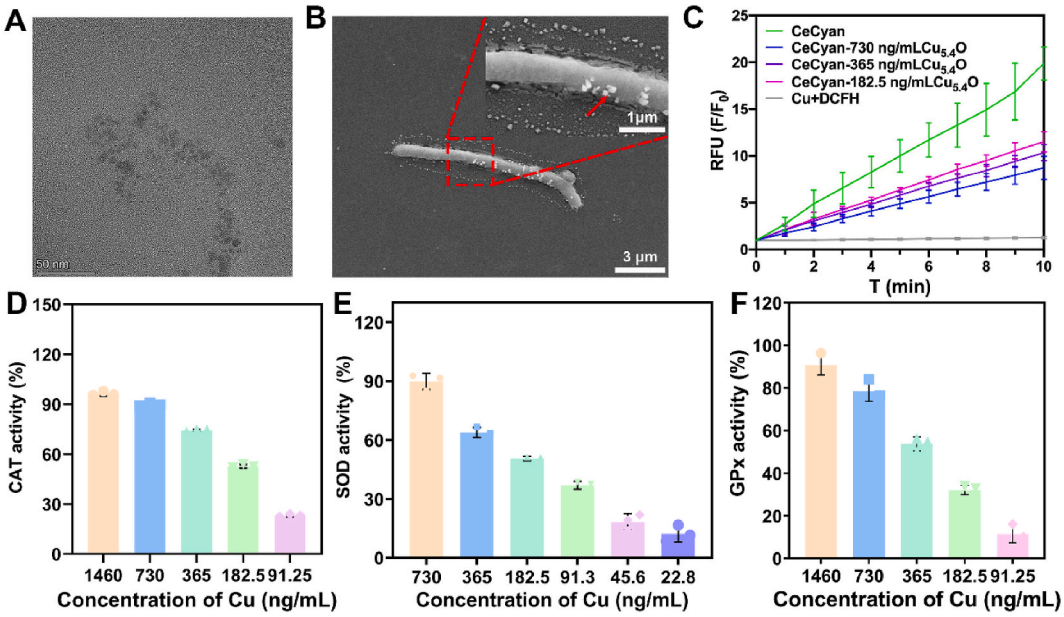


**Fig. 2.** ***In vitro*** **characterization of $Cu_{5.4}O$ USNPs and CeCyan-$Cu_{5.4}O$. (A)** TEM image of $Cu_{5.4}O$ USNPs. **(B)** SEM image of **CeCyan-$Cu_{5.4}O$. (C)** The ROS generation capacity of CeCyan-$Cu_{5.4}O$ and CeCyan through DCFH-DA method. **(D)** CAT-like, **(E)** SOD-like, and **(F)** GPx-like activity of $Cu_{5.4}O$ USNPs.

Furthermore, three kinds of main ROS related catalysis including catalase (CTA), superoxide dismutase (SOD), glutathione peroxidase (GPx) of $Cu_{5.4}O$ USNPs were also examined, respectively. As shown in Fig. 2D, E and 2F, three kinds of ROS were significantly eliminated by $Cu_{5.4}O$ USNPs in a concentration dependent manner. High CAT and SOD activities were presented when the concentration of Cu was higher than 182.5 ng/mL. At such concentration, the suppression proportions of $H_2O_2$, $\cdot O^{2-}$ and GSH were 52.7%, 50.59% and 32.12%, respectively. When the Cu concentration was 365 ng/mL, the activities of CAT, SOD and GPx reached 74.14%, 63.93% and 53.73%, respectively. Therefore, the concentration of 365 ng/mL of Cu was chosen to be loaded onto CeCyan cells in the following experiments. The generation of $O_2$ during catalytic reaction further enhanced PDT and provided $O_2$ for the tissue repair. In the immune responses caused by infection, oxidative stress and inflammation are intertwined to cause tissue damage and failure to heal. The PDT process can quickly kill bacteria by generating ROS. However, the generated free radicals also further enhance the oxidative stress and inflammatory response in the microenvironment, which is detrimental to wound tissue repair. As a result, the free radicals scavenging property of nanozymes after sterilization, coupled with the continuous oxygen production by Cyan, is considered to be a novel strategy to accelerate wound repair.

### 3.3. *Biocompatibility evaluation of CeCyan-$Cu_{5.4}O$*

GelMA hydrogel also has been used to photo-crosslink into a contact

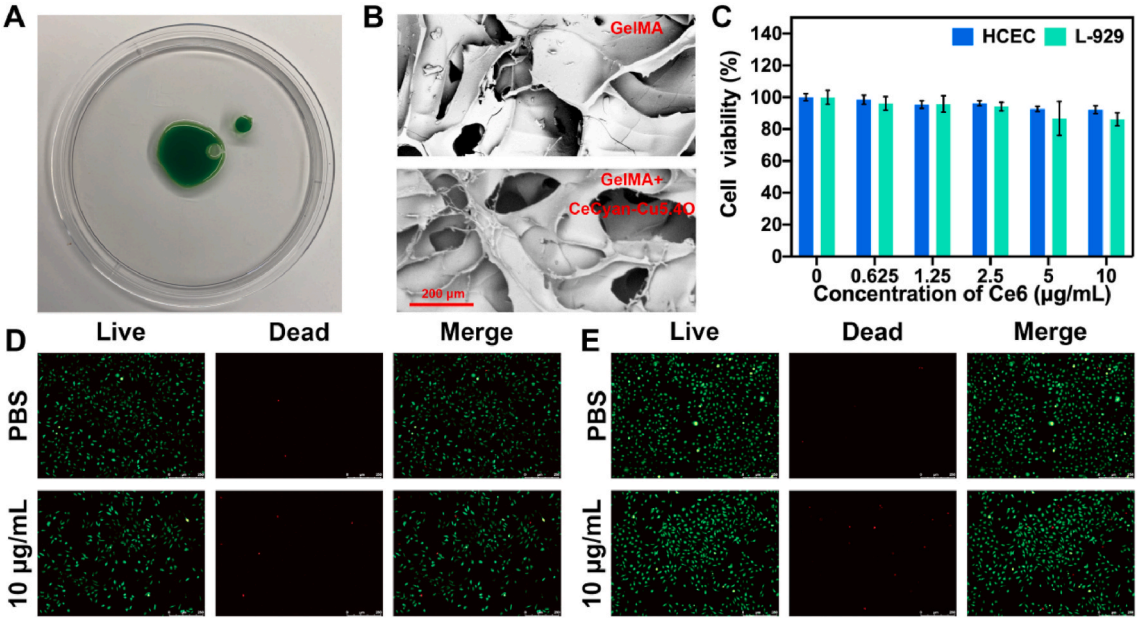


**Fig. 3.** Morphological structure and cell compatibility of CeCyan-$Cu_{5.4}O$. (A) Images of CeCyan-$Cu_{5.4}O$. (B) The cross-section SEM micrograph of GelMA hydrogel without and with CeCyan-$Cu_{5.4}O$. (C) Cell viability of L-929 and HCEC cocultured with CeCyan-$Cu_{5.4}O$ (n = 6). Representative fluorescence images of (D) HCEC and (E) L-929 cells dealt with or without CeCyan-$Cu_{5.4}O$ gel ([Ce6] = 10 μg/mL) stained by calcein-AM/PI double stained assay kit.

lens for corneal administration, and also for in situ crosslinking on the surface of the gingival infection site [52,53]. Considering the poor adhesion and the short residence time of CeCyan-$Cu_{5.4}O$ in the following anaerobic infectious keratitis and periophthalmitis, the widely recognized GelMA hydrogel with high biocompatibility and large pore size was used to encapsulate CeCyan-$Cu_{5.4}O$ [54]. Injectable GelMA hydrogel formed with 65% substitution degree of MA after photo-crosslinking (Fig. 3A and B and Fig. S4). GelMA hydrogel has a highly porous structure with a pore size of 40–143 μm, which is much larger than the size of Cyan. It is well recognized that the 3D structure with highly interconnected pores provides a favorable condition for high amount of CeCyan-$Cu_{5.4}O$ loading. The obtained microstructure also provides a suitable environment for cell penetration, oxygen diffusion and PDT function [55]. Furthermore, the gelatin in GelMA hydrogel can be degraded by matrix metalloproteinase (MMP) inflammatory responsive release of the frugs, which is highly expressed in inflammatory lesions [56]. Fig. S6 explores the exudation of $Cu_{5.4}O$ and amide-functionalized Ce6 from GelMA within 30 min of treatment. It can be seen that only a small amount of $Cu_{5.4}O$ and amide-functionalized Ce6 leaked out during the 2 min treated time, and most of them both remained after the 30 min treatment.

In this work, the Cyan themselves do not secrete toxins, and the amount of Cu is only nanograms, which do not produce toxic substances. The source of cytotoxicity may be the photosensitizer, so we increased the amount of Ce6 loading to fully explore the biocompatibility of CeCyan-$Cu_{5.4}O$ ([Ce6] = 10 μg/mL). Both L929 and HCEC were exposed to different concentration of CeCyan-$Cu_{5.4}O$ and evaluated through CCK-8 assay kit and LIVE/DEAD assay kit according to the manufacturer's instructions. After 24 h incubation, the cytocompatibility of the material was firstly examined by CCK-8 test (Fig. 3C). When the concentration of [Ce6] ≤10 μg/mL, the absorbance at 450 nm of all samples was still more than 90% of the blank group, indicating the normal cell proliferation and high biocompatibility. However, when the concentration of Ce6 was 20 μg/mL, the cell viability drops to 84% (data not shown). Figs. S7 and S8 showed the phototoxicity of CeCyan-$Cu_{5.4}O$ under therapeutic light intensity and the toxicity of light itself on HCEC and L929 cells.

The potential cytotoxicity of CeCyan-$Cu_{5.4}O$ was also evaluated by calcein-am/propidium iodide (PI) live/dead double staining assay (Fig. 3D and E). The viable cells showed green fluorescence and the dead cells showed red fluorescence. When the concentration of Ce6 in CeCyan-$Cu_{5.4}O$ was 10 μg/mL ([Cyan] = $1 \times 10^8$ cells/mL, [Cu] = 365 ng/mL), two cell lines maintained 90% of the survival ratio showing very low cytotoxicity. Even when the concentration of Ce6 in CeCyan-$Cu_{5.4}O$ was 20 μg/mL([Cyan] = $1 \times 10^8$ cells/mL, [Cu] = 365 ng/mL), the survival ratios of the two cell lines were higher than 85%. Therefore, it showed good biocompatibility of CeCyan-$Cu_{5.4}O$ within the concentration of [Ce6] ≤10 μg/mL.

### 3.4. *In vitro antibacterial evaluation of CeCyan-$Cu_{5.4}O$*

Bacteria resistance and bacterial biofilm formation lead to the failure of bacterial infection treatment, which are currently the main problems in infectious wound healing and tissue repair. In particular, unhealed

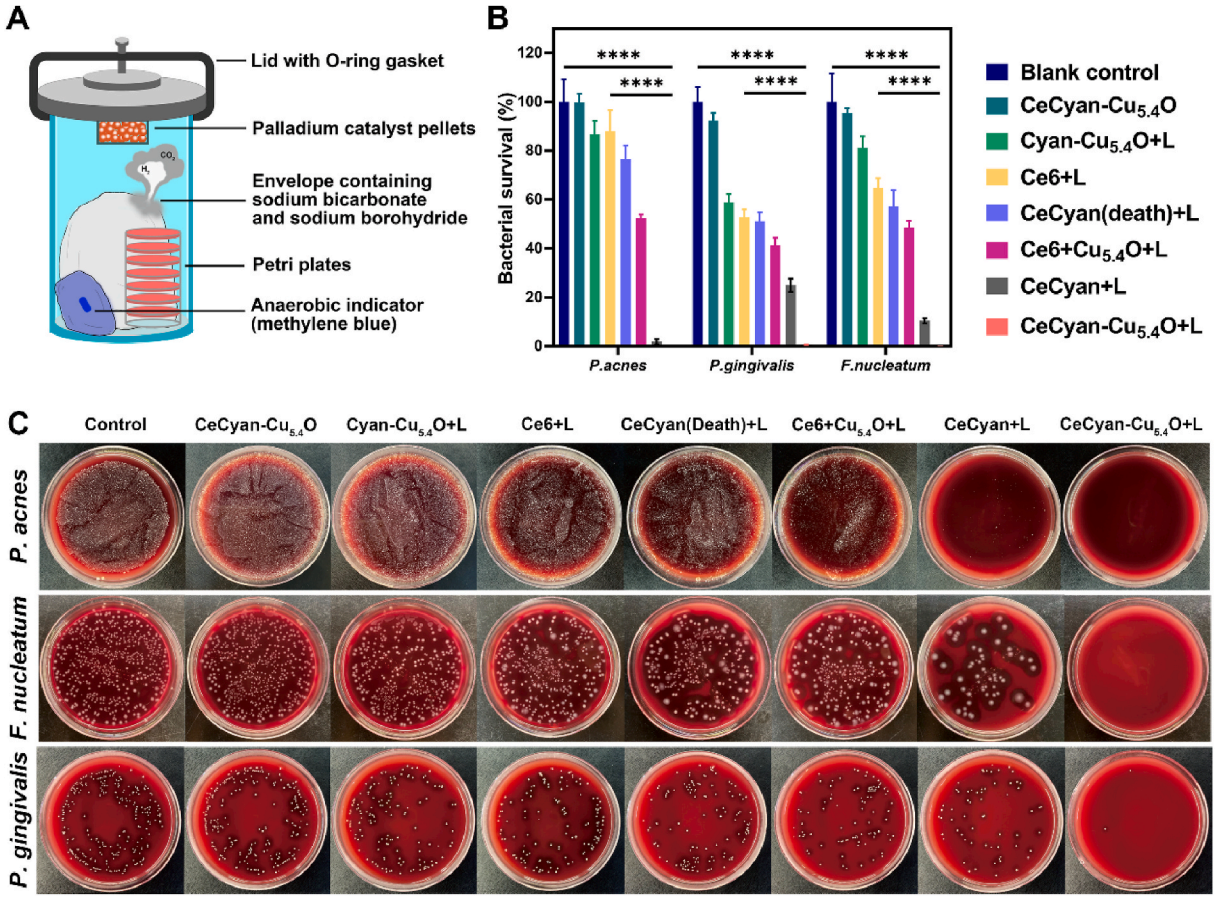


**Fig. 4.** A comparison of PDT efficacy using different photosensitizing agents under anaerobic conditions. (A) Anaerobic bacteria culture and sterilization performance test. (B) Statistical analysis number changes of *P. gingivalis, F. nucleatum* and *P. acnes* after being treated by different methods. (C) Calculating the change of *P. gingivalis, F. nucleatum* and *P. acnes* bacterial counted by dilute plate count method after being treated by different methods. The different components in each group were free Ce6 at 5 μg/mL, Ce6 in CeCyan at 5 μg/mL, Cyan at $1 \times 10^8$ CFU/mL, and $Cu_{5.4}O$ at 365 ng/mL (L means irradiated under a 660 nm laser at 200 mW/$cm^2$, 2 min) ****P < 0.0001.

wounds caused by infections lead to long-term oxidative stress damage and inflammation. For example, refractory keratitis and periodontitis are often associated with anaerobic bacteria, leading to irreversible visual damage and difficulty in gum tissue repair. PDT is a promising but oxygen-dependent developed sterilization strategy. It is worth mentioning that both Cyan under visible light and $Cu_{5.4}O$ nanozymes can provide $O_2$ to alleviate the hypoxic situation. Both *P. gingivalis* and *F. nucleatum* are widely regarded as the key pathogenic bacteria in the occurrence and development of periodontitis and plaque. While, *P. acnes* is a common pathogen causing anaerobic corneal infections and visually significant corneal ulcers.

As showed in Fig. 4A, we simulated anaerobic conditions to test the sterilization performance of the samples. After incubation with the bacteria and being treated by different strategies, the number of bacteria was calculated by plate counting method after dilution. The results in Fig. 4B, C, S9 and Fig. S10 showed that there was almost no bacterial number reduction after treated by CeCyan-$Cu_{5.4}O$ without laser irradiation and Cyan-$Cu_{5.4}O$ under irradiation, indicating the absence of ROS generation. When 5 μg/mL Ce6 was irradiated under a 660 nm laser at 200 mW/cm$^2$ for 2 min, only 20% of the bacteria was killed indicating the low bacteria killing activity. In the hypoxia environment, a large amount of nitrogen gas greatly reduced oxygen partial pressure, which led to the greatly reduction of ROS generation from Ce6 and low bactericidal property. As for the CeCyan (death)+L and Ce6+$Cu_{5.4}O$ + L groups, the generation of ROS was also not obviously enhanced due to the lack of $O_2$ production that only displayed limited bacteria killing function.

The $O_2$ production in CeCyan + L and CeCyan-$Cu_{5.4}O$ + L groups greatly enhanced the bacteria killing property in such hypoxic environment. Especially, the CeCyan-$Cu_{5.4}O$ + L group showed the unparalleled sterilization ability (100% elimination of the bacteria) to other sterilization methods. This result was in good consistency with the previous ROS production tests (Figs. 1F and 2B). Although $Cu_{5.4}O$ showed opposite effects of nanozyme-based elimination of ROS and enhanced PDT owing to the oxygen production, the presence of $Cu_{5.4}O$ overall promoted the generation of ROS. In particular, the CeCyan-$Cu_{5.4}O$ system showed a 100% killing of three kinds of bacteria just irradiated under a 660 nm laser at 200 mW/cm$^2$ for 2 min. Furthermore, the generated oxygen destroyed the low oxygen saturation environment required for the growth of anaerobic bacteria, thereby inhibiting the growth [57]. After quickly killing of bacteria, the remaining $Cu_{5.4}O$ will perform ROS eradiation function for better tissue repair, which will be further examined in the following animal experiments.

Anaerobic bacteria and bacterial biofilm are intertwined in chronic infected wounds. Due to the gradual necrosis of capillaries and nerves, the ability to kill bacteria and eliminate inflammation is further weakened, making it difficult for wounds to heal. *In vitro P. acnes*, *P. gingivalis* and *S. Gordonii* biofilm eradiation property of CeCyan-$Cu_{5.4}O$ was evaluated through 3D reconstruction of 4-day biofilm treated by different methods (Fig. 5 and Fig. S11). As shown in the live/dead bacteria image, the live bacteria in the control group are almost completely stained green. Nearly no obvious red fluorescence was observed in the control, CeCyan (death)+L, Cyan-$Cu_{5.4}O$ + L. Ce6+L and CeCyan-$Cu_{5.4}O$ groups, indicating the lack of bacteria killing function. It could be concluded that photosensitizer, oxygen production and light irradiation are the three indispensable elements for PDT function. As for the Ce6+$Cu_{5.4}O$ + L and CeCyan + L groups, obvious bacteria killing activity was observed as indicated by the large proportion of red fluorescence. However, only the CeCyan-$Cu_{5.4}O$ + L group displayed almost total eradication of the biofilm, which could be attributed to the sufficient self-oxygenation by cyanobacteria The result of anti-biofilm evaluation was consistent with that of bacteria number counting method after incubation with bacteria. Furthermore, *P. gingivalis* biofilm was much harder to eliminate than that of *P. acnes*, which might be owing to the difference in biofilm thickness and structure features, and resistance to PDT. However, it also could be found that the CeCyan-$Cu_{5.4}O$ + L group could kill all the bacteria inside the biofilm.

In an anaerobic environment, oxygen production is considered to be the decisive factor of PDT effect. In such a limited laser irradiation time (2 min), $Cu_{5.4}O$ mainly played the role of catalyzing $O_2$ production from

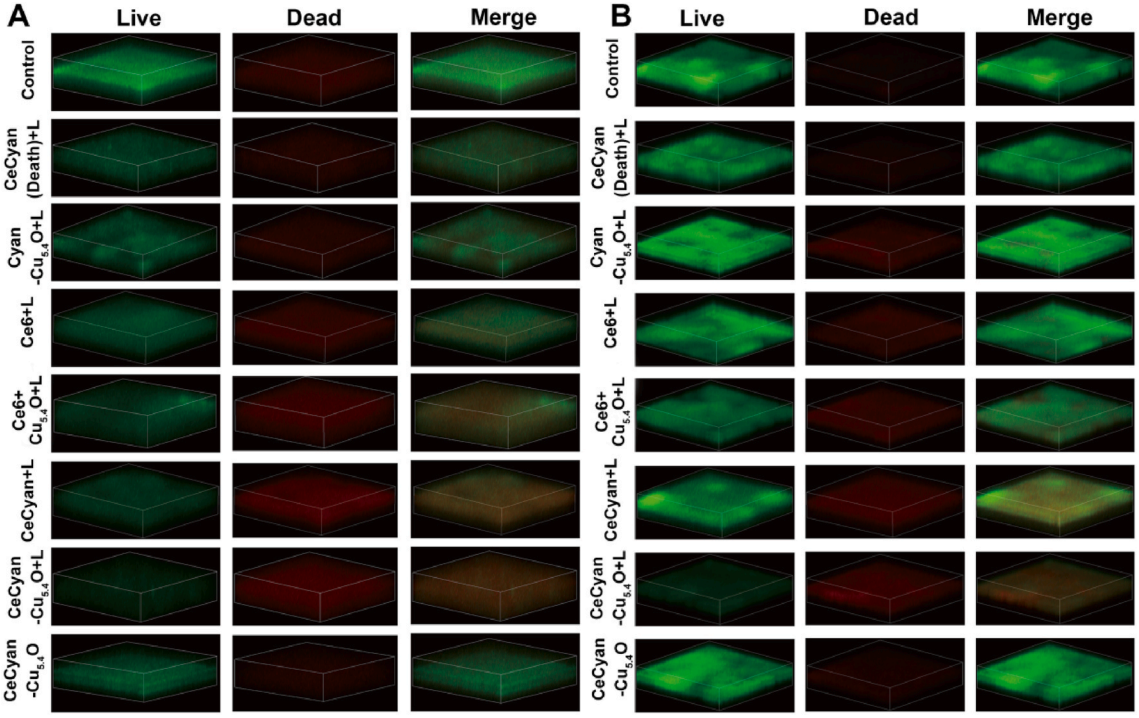


**Fig. 5.** *In vitro* biofilm eradiation evaluation of CeCyan-$Cu_{5.4}O$. The 3D reconstruction of biofilm of 4-day (A) *P. acnes* and (B) *P. gingivalis* biofilm after being treated by different method and stained by Live/Dead Baclight Bacterial Viability Kit. The different components in each group were free Ce6 at 10 μg/mL, Ce6 in CeCyan at 10 μg/mL, Cyan at 1 × 10$^8$ CFU/mL, and $Cu_{5.4}O$ at 365 ng/mL (L means irradiated under a 660 nm laser at 200 mW/cm$^2$, 2 min).

the ROS in the environment. The $O_2$ production from Cyan in only 2 min was not sufficient for PDT. As a result, CeCyan + L did not show excellent bactericidal performance. Compared with Cyan, $O_2$ production catalyzed by $Cu_{5.4}O$ nanozyme has the advantages of no nutrition and light need, and high catalytic efficiency. The results of the bacteria sterilization and the bacterial biofilm removal experiments fully proved the indispensable significance of the three components (Ce6, cyanobacteria and $Cu_{5.4}O$) especially for anaerobic infection treatment.

### 3.5. *In vivo* elimination of anaerobic infection and tissue repair

Based on the *in vitro* findings, the anaerobic infectious animal models were used to verify the therapeutic effects of CeCyan-$Cu_{5.4}O$ through blending with GelMA hydrogels for better wound filling and long-term retention time. Both anaerobic infectious keratitis and periodontitis animal models were established after adaptive feeding for one week. The corneal epithelium of rats was scraped off and the anterior stroma was infiltrated with bacteria to establish a corneal infection model. Rats were injected with LPS and periodontal mixed bacteria to establish a periodontal infection model. Corneal infected rats wore contact lenses made of GelMA hydrogel wrapped with different antibacterial agents every day for 2 min irradiation (660 nm, 200 mW/cm$^2$) and another 30 min wearing before removing of the contact lenses. As for the treatment of infectious periodontitis, GelMA solution containing different antibacterial agents was injected into the infected site every day for light cross-linking. After 2 min irradiating with a 660 nm laser (200 mW/cm$^2$), the hydrogel was removed by PBS.

As shown in Fig. 6A, obvious turbidity in the cornea was observed after the construction of anaerobic infectious keratitis model. Corneal defect was clearly visible in the fluorescence image as indicated by the asterisk. At Day 3, the cornea in the CeCyan-$Cu_{5.4}O$ + L group had basically recovered to be transparent, indicating the basic regression of inflammation. In comparison, the turbid area of cornea in the CeCyan + L and Levofloxacin groups also showed obvious reduction compared with Day 1. On the contrary, the cornea in the control group still showed large opaque areas, which was still in the stage of severe bacterial infection and inflammation. At the end of 3 days treatment, the number of surviving bacteria in the infected tissues was evaluated by the plate coating method (Fig. 6B). There was almost no living bacteria in the wound treated by CeCyan-$Cu_{5.4}O$ + L, which certified the high efficiency of PDT against anaerobic bacteria infection. Compromised anaerobic bacteria killing function was also observed in CeCyan + L and Levofloxacin groups. The wound in the control group demonstrated serious bacterial infection and large number of living bacteria. As for the clinical score of inflammation [58], after 3 days treatment, the score of CeCyan-$Cu_{5.4}O$ + L decreased more faster than those in the other groups (Fig. 6C and Fig. S12). As a result, the excellent bactericidal property of CeCyan-$Cu_{5.4}O$ could be attributed to the self-oxygenated enhanced PDT and light transmittance of corneal tissue. The fast inflammation elimination function of CeCyan-$Cu_{5.4}O$ should be attributed to the ROS catalytic degradation ability of $Cu_{5.4}O$ after bacteria killing.

The inflammatory cell infiltration and related inflammatory factor

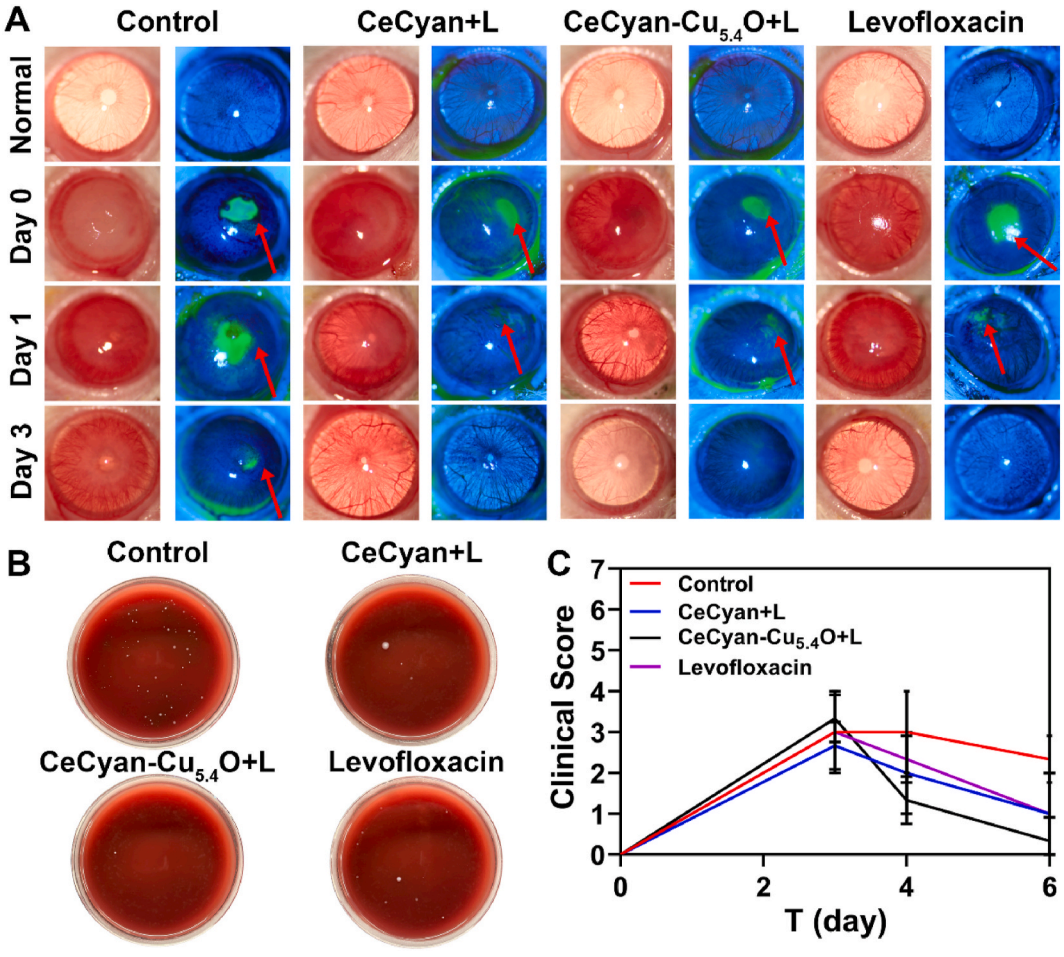


**Fig. 6.** *In vivo* bacteria killing and inflammation elimination of CeCyan-$Cu_{5.4}O$ in anaerobic infectious keratitis model. (A) The cornea slit lamp observation after different antibacterial treatments (CeCyan + L, CeCyan-$Cu_{5.4}O$ + L and Levofloxacin) compared to the control without any treatment. (B) The coating of fluid from the infected corneal tissues cultured on agar plates. (C) The inflammation clinical score of corneas after different antibacterial treatments. ([Ce6] = 10 μg/mL, Cyan = 1 × 10$^8$ CFU/mL, Cu = 365 ng/mL. Levofloxacin: 0.5 wt%, 10 μL, twice a day, L means irradiated under a 660 nm laser at 200 mW/cm$^2$, 2 min).

expression were also tested through H&E staining and immunofluorescence (Fig. 7). Inflammatory infiltration is the most direct evidence of the inflammatory response state, and it is positively related to the number of inflammatory cells. Under normal conditions, the cornea is in an immune-exempt state to reduce inflammatory cell infiltration for high light transmittance. Therefore, the inflammatory response, including the expression of inflammatory factors and related inflammatory cell infiltration, needs to be promptly eliminated from the visual pathway damage caused by the inflammatory response after sterilization. As observed in Fig. 7A, the cornea with anaerobic infection was significantly infiltrated by immune cells such as macrophages, neutrophils, *etc*. However, the inflammatory infiltration into cornea was significantly reduced after CeCyan + L, Levofloxacin or CeCyan-$Cu_{5.4}O$ + L treatment. In particular, CeCyan-$Cu_{5.4}O$ + L group exhibited the lowest number of inflammatory cells and inflammatory response. As for the immunofluorescence of three kinds of infection-related inflammatory factors including TNF-$\alpha$, IL-6 and IL-1β, the control cornea tissue displayed strong green fluorescent signal suggesting the presence of a large number of inflammatory factors (Fig. 7B, C and 7D). Both Levofloxacin or CeCyan-$Cu_{5.4}O$ + L groups showed significant reduction of inflammatory factors levels.

Anaerobic infectious periodontitis model is another representative anaerobic bacterial infection model and mostly mixed infection with multiple bacteria (Fig. 8). As shown in Fig. 8A, the periodontitis animal model showed obvious gingival edema after construction of the animal model. Then, different treatment was applied to the bacterial infection areas. On Day 3, both CeCyan-$Cu_{5.4}O$ + L and Levofloxacin groups showed basically elimination of the edema. In addition, the tiny blood supply at the infected site gradually recovered, and the gums became transparent. However, there was still some edema and internal bleeding in the CeCyan + L group, and the gums did not turn to transparent. In the control group, the inflammation became more severe with the increase of area and degree of edema. It also could be found that CeCyan-$Cu_{5.4}O$ + L completely killed all bacteria under laser irradiation for 2 min. There was partial suppuration, and the gums completely lost transparent and appeared porcelain white. The H&E staining (Fig. 8B) and immunofluorescence (Fig. S13) also displayed greatly reduction of inflammation after bacterial infection elimination, which could be owing to the nanozyme catalytic activity of $Cu_{5.4}O$ USNPs in ROS elimination. Expression of IL-1 β and TNF-α mRNA more directly showed the level of inflammatory factors in gingival tissues after being treated by different methods (Fig. 8C and D). The CeCyan-$Cu_{5.4}O$ + L strategy had the lowest inflammation and the optimal tissue repair ability, which further proved the efficiency and superiority of this strategy.

## 4. Conclusion

A formulation has been developed involving both a photosensitizer and cyanobacteria for promoting efficacy of PDT in a relatively hypoxic environment. This is shown to enhance eradication of biofilm *in vitro* and in a rat model by providing a supply of oxygen which is a necessary factor in photokilling. Under laser irradiation, the photosensitizer Ce6 combined with cyanobacteria achieves the same electron transfer effect with only one-tenth of the original dose. In the treatment of anaerobic infections, the production of oxygen is the key factor to enhance PDT effect. Furthermore, $Cu_{5.4}O$ USNPs displayed multiple ROS scavenging activity including CAT, SOD and GPx, also leading to the oxygen generation. In this strategy, the rapid sterilization, biofilm removal under light and then efficient removal of ROS is realized by adjusting the ratio of Ce6 and $Cu_{5.4}O$ USNPs. The CeCyan-$Cu_{5.4}O$ showed good

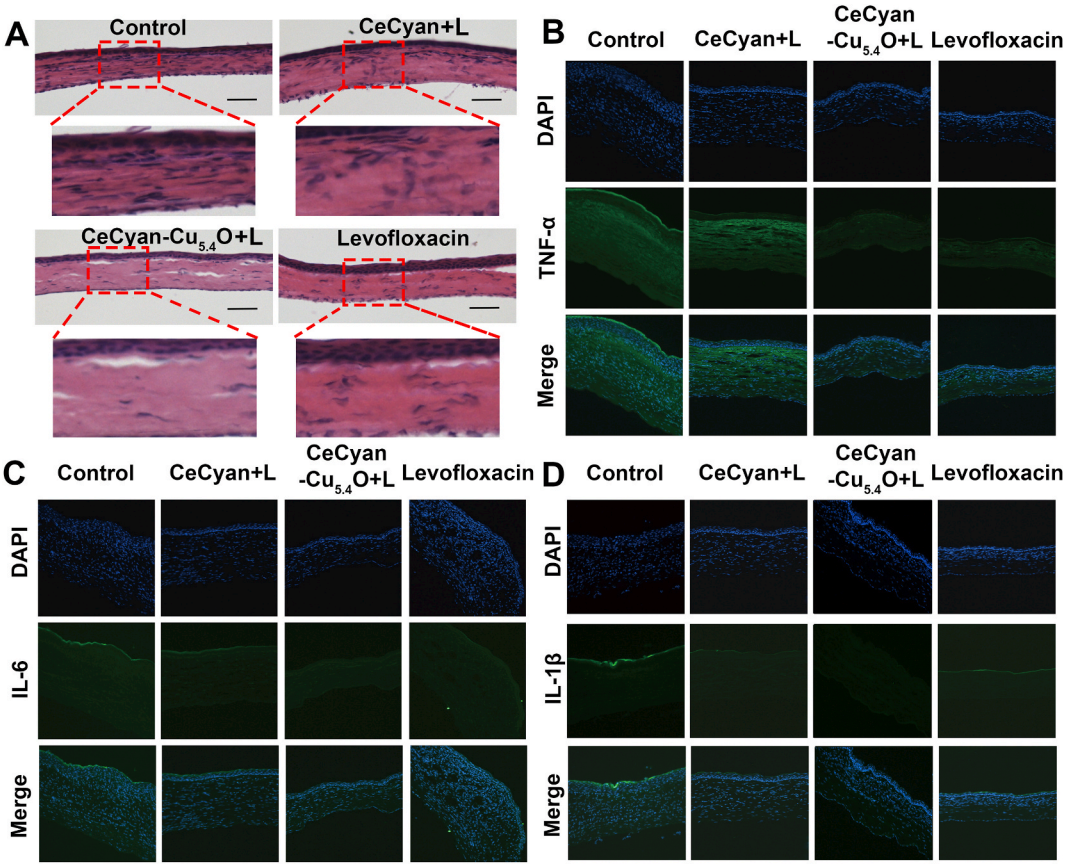


**Fig. 7.** Inflammatory changes in the anaerobic infectious keratitis after being treated. (A) H&E stained micrographs of corneal tissues after different treatments (scale bar = 100 μm). Micrographs of fluorescence immunostaining analysis of (B)TNF-α, (C) IL-6 and (D) IL-1β after being treated by different methods. ([Ce6] = 10 μg/mL, Cyan = $1 \times 10^8$ CFU/mL, Cu = 365 ng/mL. L means irradiated under a 660 nm laser at 200 mW/$cm^2$, 2 min).

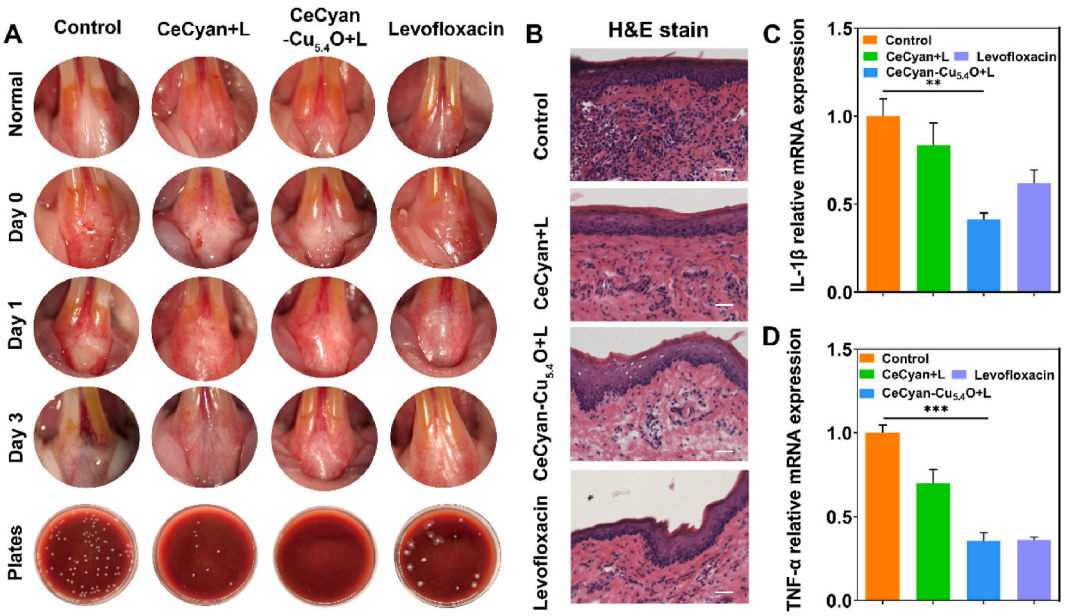


**Fig. 8.** *In vivo* bacteria killing and inflammation elimination of CeCyan-$Cu_{5.4}O$ in anaerobic infectious periodontitis model. (A) The intraoral slit lamp pictures under different treatments (CeCyan + L, CeCyan-$Cu_{5.4}O$ + L, and Levofloxacin) compared to the control group. And the bacteria separated from gingival tissues were cultured on agar plates. (B) H&E stained micrographs of periodontal tissues after different treatments (scale bar = 100 μm). (C) IL-1 β and (D) TNF-α mRNA expression in gingival tissues after being treated by different methods. ([Ce6] = 10 μg/mL, Cyan = $1 \times 10^8$ CFU/mL, Cu = 365 ng/mL. L means irradiated under a 660 nm laser at 200 mW/$cm^2$, 2 min) **P < 0.01, ***P < 0.001.

biocompatibility within the concentration of [Ce6] ≤10 μg/mL. Both bactericidal activity and biofilm removal tests demonstrated the excellent antibacterial function (about 100% killing of the anaerobic bacteria). Both anaerobic infectious keratitis and infectious periodontitis animal models proved the superiority of the self-produced oxygen PDT system in anaerobic infection treatment and tissue repair.

## CRediT authorship contribution statement

**Bailiang Wang:** Writing – original draft, completed material preparation and wrote the manuscript. **Yishun Guo:** did antibacterial and cell testing. **Hanwen Guo:** did antibacterial and cell testing. **Yiming Zhong:** completed animal experiment part and revised the manuscript. **Xiaomin Huang:** did antibacterial and cell testing. **Yifan Ge:** did antibacterial and cell testing. **Qingying Wang:** completed animal experiment part and revised the manuscript. **Xiaoying Chu:** completed animal experiment part and revised the manuscript. **Yingying Jin:** completed animal experiment part and revised the manuscript. **Kaiyue Lan:** completed animal experiment part and revised the manuscript. **Mei Yang:** designed the work and revised the manuscript. **Jia Qu:** designed the work and revised the manuscript. All of the authors participate in the experiments or writing work.

## Declaration of competing interest

The authors claim no conflicts of interest.

## Acknowledgments

This work was supported by the National Natural Science Foundation of China (31771026, 82072077), Zhejiang Provincial Natural Science Foundation of China (LR19H180001), Project of State Key Laboratory of Ophthalmology, Optometry and Visual Science, Wenzhou Medical University (J02-20190203), Wenzhou key program of scientific and technological innovation (ZY2019017), Engineering Research Center of Clinical Functional Materials and Diagnosis & Treatment Devices of Zhejiang Province (WIUCASK19005) which are greatly acknowledged.

## Appendix A. Supplementary data

Supplementary data to this article can be found online at https://doi.org/10.1016/j.bioactmat.2021.10.032.

## References

[1] Z.Q. Zhu, Q. Gao, Z.Y. Long, Q.Y. Huo, Y.F. Ge, N. Vianney, N.A. Daliko, Y.C. Meng, J. Qu, H. Chen, B.L. Wang, Polydopamine/poly(sulfobetaine methacrylate) Co-deposition coatings triggered by CuSO4/H2O2 on implants for improved surface hemocompatibility and antibacterial activity, Bioact Mater 6 (8) (2021) 2546–2556.
[2] H.L. Yawei Ren, Xiangmei Liu, Yufeng Zheng, Zhaoyang Li, Changyi Li, S.Z. Kelvin, Wai Kwok Yeung, Yanqin Liang, Zhenduo cui, and shuilin Wu, photoresponsive materials for antibacterial applications, Cell Reports Physical Science 1 (11) (2021) 30.
[3] J.H. Huang, M.Y. Yu, W.J. Yin, B. Liang, A. Li, J.F. Li, X.L. Li, S.C. Zhao, F. Liu, Development of a novel RNAi therapy: engineered miR-31 exosomes promoted the healing of diabetic wounds, Bioact Mater 6 (9) (2021) 2841–2853.
[4] D.X. Li, T. Chen, Y.F. Zhang, Y.H. Xu, H.T. Niu, Synergistical starvation and chemodynamic therapy for combating multidrug-resistant bacteria and accelerating diabetic wound healing, Adv Healthc Mater (2021) 2100716.
[5] T. Wang, Y.R. Li, E.J. Cornel, C. Li, J.Z. Du, Combined antioxidant-antibiotic treatment for effectively healing infected diabetic wounds based on polymer vesicles, ACS Nano 15 (5) (2021) 9027–9038.
[6] C. Dunnill, T. Patton, J. Brennan, J. Barrett, M. Dryden, J. Cooke, D. Leaper, N. T. Georgopoulos, Reactive oxygen species (ROS) and wound healing: the functional role of ROS and emerging ROS-modulating technologies for augmentation of the healing process, Int. Wound J. 14 (1) (2017) 89–96.
[7] S.T. LoPresti, B. Popovic, M. Kulkarni, C.D. Skillen, B.N. Brown, Free radical-decellularized tissue promotes enhanced antioxidant and anti-inflammatory macrophage response, Biomaterials 222 (2019) 119376.
[8] S. Reuter, S.C. Gupta, M.M. Chaturvedi, B.B. Aggarwal, Oxidative stress, inflammation, and cancer: how are they linked? Free Radic. Biol. Med. 49 (11) (2010) 1603–1616.
[9] U.Z. Paracha, K. Fatima, M. Alqahtani, A.C. haudhary, I. Qadri, Oxidative stress and hepatitis C virus, Virol. J. 10 (1) (2013) 251.
[10] S.A. Eming, P. Martin, M. Tomic-Canic, Wound repair and regeneration: mechanisms, signaling, and translation, Sci. Transl. Med. 6 (265) (2014) 265sr6.
[11] L. Sun, W.Y. Jiang, H.R. Zhang, Y.S. Guo, W. Chen, Y.Y. Jin, H. Chen, K.H. Du, H. D. Dai, J. Ji, B.L. Wang, Photosensitizer-loaded multifunctional chitosan nanoparticles for simultaneous in situ imaging, highly efficient bacterial biofilm eradication, and tumor ablation, Acs Appl Mater Inter 11 (2) (2019) 2302–2316.
[12] Y.Q. Wang, Y.Y. Jin, W. Chen, J.J. Wang, H. Chen, L. Sun, X. Li, J. Ji, Q. Yu, L. Y. Shen, B.L. Wang, Construction of nanomaterials with targeting phototherapy properties to inhibit resistant bacteria and biofilm infections, Chem. Eng. J. 358 (2019) 74–90.

[13] S.A. Khan, C.S. Lee, Recent progress and strategies to develop antimicrobial contact lenses and lens cases for different types of microbial keratitis, Acta Biomater. 113 (2020) 101–118.
[14] N.V. Prajna, N. Radhakrishnan, P. Lalitha, A. Austin, K.J. Ray, J.D. Keenan, T. C. Porco, T.M. Lietman, J. Rose-Nussbaumer, Cross-linking-assisted infection reduction A randomized clinical trial evaluating the effect of adjuvant cross-linking on outcomes in fungal keratitis, Ophthalmology 127 (2) (2020) 159–166.
[15] X.K. Ding, S. Duan, X.J. Ding, R.H. Liu, F.J. Xu, Versatile antibacterial materials: an emerging arsenal for combatting bacterial pathogens, Adv. Funct. Mater. 28 (40) (2018) 1802140.
[16] Y.C. Yang, P. He, Y.X. Wang, H.T. Bai, S. Wang, J.F. Xu, X. Zhang, Supramolecular radical anions triggered by bacteria in situ for selective photothermal therapy, Angew. Chem. Int. Ed. 56 (51) (2017) 16239–16242.
[17] B.H. Hu, C. Berkey, T. Feliciano, X.H. Chen, Z.Y. Li, C. Chen, S. Amini, M.H. Nai, Q. L. Lei, R. Ni, J. Wang, W.R. Leow, S.W. Pan, Y.Q. Li, P.Q. Cai, A. Miserez, S.Z. Li, C. T. Lim, Y.L. Wu, T.W. Odom, R.H. Dauskardt, X.D. Chen, Thermal-disrupting interface mitigates intercellular cohesion loss for accurate topical antibacterial therapy, Adv. Mater. 32 (12) (2020) 1907030.
[18] B.L. Wang, Q.W. Xu, Z. Ye, H.H. Liu, Q.K. Lin, K.H. Nan, Y.Z. Li, Y. Wang, L. Qi, H. Chen, Copolymer brushes with temperature-triggered, reversibly switchable bactericidal and antifouling properties for biomaterial surfaces, Acs Appl Mater Inter 8 (40) (2016) 27207–27217.
[19] A.F. Bakuzis, Nanomedicine and thermal therapies: where are we going? Int. J. Hyperther. 37 (3) (2020) 1–3.
[20] J. Tian, B. Huang, M.H. Nawaz, W. Zhang, Recent advances of multi-dimensional porphyrin-based functional materials in photodynamic therapy, Coord. Chem. Rev. 420 (2020) 213410.
[21] J. Tian, W. Zhang, Synthesis, self-assembly and applications of functional polymers based on porphyrins, Prog. Polym. Sci. 95 (2019) 65–117.
[22] Y.J. Jiang, M. Han, Y. Bo, Y.J. Feng, W.M. Li, J.R. Wu, Z.Y. Song, Z.H. Zhao, Z. Z. Tan, Y.Y. Chen, T.R. Xue, Z.H. Fu, S.H. Kuo, G.W. Lau, E. Luijten, J.J. Cheng, Metaphilic" cell-penetrating polypeptide-vancomycin conjugate efficiently eradicates intracellular bacteria via a dual mechanism, Acs Central Sci 6 (12) (2020) 2267–2276.
[23] W. Qin, C.Y. Wang, Y.X. Ma, M.J. Shen, J. Li, K. Jiao, F.R. Tay, L.N. Niu, Microbe-mediated extracellular and intracellular mineralization: environmental, industrial, and biotechnological applications, Adv. Mater. 32 (22) (2020) 1907833.
[24] B.H. Gan, J. Gaynord, S.M. Rowe, T. Deingruber, D.R. Spring, The multifaceted nature of antimicrobial peptides: current synthetic chemistry approaches and future directions, Chem. Soc. Rev. 50 (13) (2021) 7820–7880.
[25] J.J. Huo, Q.Y. Jia, H. Huang, J. Zhang, P. Li, X.C. Dong, W. Huang, Emerging photothermal-derived multimodal synergistic therapy in combating bacterial infections, Chem. Soc. Rev. 32 (22) (2021) 1907833.
[26] H. Chen, J. Yang, L. Sun, H.R. Zhang, Y.S. Guo, J. Qu, W.Y. Jiang, W. Chen, J. Ji, Y. W. Yang, B.L. Wang, Synergistic chemotherapy and photodynamic therapy of endophthalmitis mediated by zeolitic imidazolate framework-based drug delivery systems, Small 15 (47) (2019) 1903880.
[27] X. Li, S. Yu, Y. Lee, T. Guo, N. Kwon, D. Lee, S.C. Yeom, Y. Cho, G. Kim, J.D. Huang, S. Choi, K.T. Nam, J. Yoon, Vivo albumin traps photosensitizer monomers from self-assembled phthalocyanine nanovesicles: a facile and switchable theranostic approach, J. Am. Chem. Soc. 141 (3) (2019) 1366–1372.
[28] F. Yu, C. Chen, G. Yang, Z. Ren, H. Cao, L. Zhang, W. Zhang, An acid-triggered porphyrin-based block copolymer for enhanced photodynamic antibacterial efficacy, Sci. China Chem. 64 (3) (2021) 459–466.
[29] X.L. Sun, J. Sun, Y. Sun, C.Y. Li, J. Fang, T.S. Zhang, Y. Wan, L. Xu, Y.M. Zhou, L. Wang, B. Dong, Oxygen self-sufficient nanoplatform for enhanced and selective antibacterial photodynamic therapy against anaerobe-induced periodontal disease, Adv. Funct. Mater. 31 (20) (2021) 2101040.
[30] L. Tan, J. Li, X.M. Liu, Z.D. Cui, X.J. Yang, S.L. Zhu, Z.Y. Li, X.B. Yuan, Y.F. Zheng, K.W.K. Yeung, H.B. Pan, X.B. Wang, S.L. Wu, Rapid biofilm eradication on bone implants using red phosphorus and near-infrared light, Adv. Mater. 30 (31) (2018) 1801808.
[31] X. Li, D. Lee, J.D. Huang, J. Yoon, Phthalocyanine-assembled nanodots as photosensitizers for highly efficient type I photoreactions in photodynamic therapy, Angew Chem. Int. Ed. Engl. 57 (31) (2018) 9885–9890.
[32] X.C. Cai, Z.X. Xie, B.B. Ding, S. Shao, S. Liang, M.L. Pang, J. Lin, Monodispersed copper(I)-Based nano metal-organic framework as a biodegradable drug carrier with enhanced photodynamic therapy efficacy, Adv. Sci. 6 (15) (2019) 1900848.
[33] Y. Cheng, X.P. Kong, Y. Chang, Y.L. Feng, R.X. Zheng, X.Q. Wu, K.Q. Xu, X.F. Gao, H.Y. Zhang, Spatiotemporally synchronous oxygen self-supply and reactive oxygen species production on Z-scheme heterostructures for hypoxic tumor therapy, Adv. Mater. 32 (11) (2020) 1908109.
[34] L.C. He, Q.Q. Ni, J. Mu, W.P. Fan, L. Liu, Z.T. Wang, L. Li, W. Tang, Y.J. Liu, Y. Y. Cheng, L.G. Tang, Z. Yang, Y. Liu, J.H. Zou, W.J. Yang, O. Jacobson, F. Zhang, P. T. Huang, X.Y. Chen, Solvent-assisted self-assembly of a metal-organic framework based biocatalyst for cascade reaction driven photodynamic therapy, J. Am. Chem. Soc. 142 (14) (2020) 6822–6832.
[35] Y. Qiao, F. Yang, T.T. Xie, Z. Du, D.N. Zhong, Y.C. Qi, Y.Y. Li, W.L. Li, Z.M. Lu, J. H. Rao, Y. Sun, M. Zhou, Engineered algae: a novel oxygen-generating system for effective treatment of hypoxic cancer, Sci Adv 6 (21) (2020), eaba5996.
[36] D.F. Hu, L.Y. Zou, W.J. Yu, F. Jia, H.J. Han, K. Yao, Q. Jin, J. Ji, Relief of biofilm hypoxia using an oxygen nanocarrier: a new paradigm for enhanced antibiotic therapy, Adv. Sci. 7 (12) (2020) 2000398.
[37] X.F. Wang, M.L. Li, Q.Q. Fang, W.Y. Zhao, D. Lou, Y.Y. Hu, J. Chen, X.Z. Wang, W. Q. Tan, Flexible electrical stimulation device with Chitosan-Vaseline (R) dressing accelerates wound healing in diabetes, Bioact Mater 6 (1) (2021) 230–243.
[38] A.U.R. Khan, K. Huang, M.S. Khalaji, F. Yu, X.R. Xie, T.H. Zhu, Y. Morsi, J.Z. Zhao, X.M. Mo, Multifunctional bioactive core-shell electrospun membrane capable to terminate inflammatory cycle and promote angiogenesis in diabetic wound, Bioact Mater 6 (9) (2021) 2783–2800.
[39] R.M. Haley, H.A. von Recum, Localized and targeted delivery of NSAIDs for treatment of inflammation: a review, Exp. Biol. Med. 244 (6) (2019) 433–444.
[40] A. Shukla, R.C. Fuller, P.T. Hammond, Design of multi-drug release coatings targeting infection and inflammation, J. Contr. Release 155 (2) (2011) 159–166.
[41] M. Chang, T.T. Nguyen, Strategy for treatment of infected diabetic foot ulcers, Accounts Chem. Res. 54 (5) (2021) 1080–1093.
[42] L.W. Wang, X. Zhang, X. Yu, E.N. Gao, Z.Y. Shen, X.L. Zhang, S.G. Ge, J. Liu, Z. J. Gu, C.Y. Chen, An all-organic semiconductor C3N4/PDINH heterostructure with advanced antibacterial photocatalytic therapy activity, Adv. Mater. 31 (33) (2019) 1901965.
[43] L. Ma, F.B. Jiang, X. Fan, L.Y. Wang, C. He, M. Zhou, S. Li, H.R. Luo, C. Cheng, L. Qiu, Metal-organic-framework-engineered enzyme-mimetic catalysts, Adv. Mater. 32 (49) (2020) 2003065.
[44] Q. Wang, J. Jiang, L.Z. Gao, Nanozyme-based medicine for enzymatic therapy: progress and challenges, Biomed. Mater. 16 (4) (2021), 042002.
[45] Z.R. Wang, R.F. Zhang, X.Y. Yan, K.L. Fan, Structure and activity of nanozymes: inspirations for de novo design of nanozymes, Mater. Today 41 (2020) 81–119.
[46] T.F. Liu, B.W. Xiao, F. Xiang, J.L. Tan, Z. Chen, X.R. Zhang, C.Z. Wu, Z.W. Mao, G. X. Luo, X.Y. Chen, J. Deng, Ultrasmall copper-based nanoparticles for reactive oxygen species scavenging and alleviation of inflammation related diseases, Nat. Commun. 11 (1) (2020) 2788.
[47] C.J. Knoot, J. Ungerer, P.P. Wangikar, H.B. Pakrasi, Cyanobacteria: promising biocatalysts for sustainable chemical production, J. Biol. Chem. 293 (14) (2018) 5044–5052.
[48] M.F. Huo, L.Y. Wang, L.L. Zhang, C.Y. Wei, Y. Chen, J.L. Shi, Photosynthetic tumor oxygenation by photosensitizer-containing cyanobacteria for enhanced photodynamic therapy, Angew. Chem. Int. Ed. 59 (5) (2020) 1906–1913.
[49] H. Kowata, S. Tochigi, H. Takahashi, S. Kojima, Outer membrane permeability of cyanobacterium synechocystis sp strain PCC 6803: studies of passive diffusion of small organic nutrients reveal the absence of classical porins and intrinsically low permeability, J. Bacteriol. 199 (19) (2017) e00371-17.
[50] S.J. Gao, X.Z. Yan, G.C. Xie, M. Zhu, X.Y. Ju, P.J. Stang, Y. Tian, Z.W. Niu, Membrane intercalation-enhanced photodynamic inactivation of bacteria by a metallacycle and TAT-decorated virus coat protein, P Natl Acad Sci USA 116 (47) (2019) 23437–23443.
[51] Y.Y. Huang, J.S. Ren, X.G. Qu, Nanozymes: classification, catalytic mechanisms, activity regulation, and applications, Chem. Rev. 119 (6) (2019) 4357–4412.
[52] B. Kong, Y. Chen, R. Liu, X. Liu, C.Y. Liu, Z.W. Shao, L.M. Xiong, X.N. Liu, W. Sun, S.L. Mi, Fiber reinforced GelMA hydrogel to induce the regeneration of corneal stroma, Nat. Commun. 11 (1) (2020) 1435.
[53] S. Ansari, P. Sarrion, M.M. Hasani-Sadrabadi, T. Aghaloo, B.M. Wu, A. Moshaverinia, Regulation of the fate of dental-derived mesenchymal stem cells using engineered alginate-GelMA hydrogels, J. Biomed. Mater. Res. 105 (11) (2017) 2957–2967.
[54] J.S. Ribeiro, E.A.F. Bordini, J.A. Ferreira, L. Mei, N. Dubey, J.C. Fenno, E. Piva, R. G. Lund, A. Schwendeman, M.C. Bottino, Injectable MMP-responsive nanotube-modified gelatin hydrogel for dental infection ablation, Acs Appl Mater Inter 12 (14) (2020) 16006–16017.
[55] Y.T. Zhu, Q. Zhang, X.L. Shi, D. Han, Hierarchical hydrogel composite interfaces with robust mechanical properties for biomedical applications, Adv. Mater. 31 (45) (2019) 1804950.
[56] D. Loessner, C. Meinert, E. Kaemmerer, L.C. Martine, K. Yue, P.A. Levett, T.J. Klein, F.P.W. Melchels, A. Khademhosseini, D.W. Hutmacher, Functionalization, preparation and use of cell-laden gelatin methacryloyl-based hydrogels as modular tissue culture platforms, Nat. Protoc. 11 (4) (2016) 727–746.
[57] Z. Lu, J.A. Imlay, When anaerobes encounter oxygen: mechanisms of oxygen toxicity, tolerance and defence, Nat. Rev. Microbiol. (2021), 1740-1526.
[58] L.D. Hazlett, M.M. Moon, M. Strejc, R.S. Berk, Evidence for N-acetylmannosamine as an ocular receptor for P. aeruginosa adherence to scarified cornea, Investig. Ophthalmol. Vis. Sci. 28 (12) (1987) 1978.